International Journal of Applied Geospatial Research
Volume 14 • Issue 1

Spatiotemporal Monitoring of Land Reclamation in the Southeastern Desert, Upper Egypt Using Satellite Data and GIS

Mostafa K. Mosleh, Department of Geography, Faculty of Arts, South Valley University, Qena, Egypt*
Khaled Hazaymeh, Department of Geography, Geoinformatics Lab. Yarmouk University, Irbid, Jordan
https://orcid.org/0000-0002-2162-7385

ABSTRACT

The objective of this study was to monitor the reclamation development and assess the LULC changes in a reclaimed area in Upper Egypt. GIS and remote sensing-based multi-temporal Landsat imageries (i.e., Landsat-5 and Landsat-8; 30m) were utilized for mapping and analyzing the spatiotemporal dynamics between 2005 to 2020. Both supervised-based maximum likelihood classifier (MLC) and normalized difference vegetation index (NDVI)-based thresholds were implemented. The results of both methods were cross-compared and showed that the agriculture activities started in 2004 with small and sparse agriculture patches. The bare land occupied more than 65.1% of the total area between 2005-2008. Overall, using the MLC and NDVI-based classification, the authors observed an increase of approximately 455.6% (17,027.7 ha) and 477.2% (16,973.5 ha) over 15 years (2005-2020), respectively. The results could be very useful for assessing the success of the Egyptian strategies to sustain the agricultural land areas and food production through horizontal expansion and investment in the desert areas.

KEYWORDS

Agriculture, Food Security, GIS, Land Use/Land Cover, NDVI, Remote Sensing

INTRODUCTION

Throughout the world's progressive history and exponential population growth, agriculture has been associated with the cultivation of land to satisfy humans' ample needs for food, fabrics, energy, and a source of income. It plays a fundamental role to sustain livelihood and economic system of any country. For instance, it composes approximately 27.2% of employment rate and contributed to ~ 68% of the global added value reaching USD $3.4 trillion in 2018 (World Bank, 2020; FAO, 2020). Furthermore, in 2018 agriculture contributed to 4% of global gross domestic product (GDP) as well as ~25% for developing countries (World Bank, 2021).

Globally, in 2018, ~ 4.8 billion hectares (ha) was accounted as arable land and ~1.6 billion ha was used for cropland, with irrigated area of 340 million ha (FAO, 2020). Croplands render major

DOI: 10.4018/IJAGR.323186 *Corresponding Author

shares of the global food supply with approximately 99.7% of all human food calories as well as 80% of all food proteins and fats for human sustainability (Pimentel & Burgess, 2013). However, there is still a global concern on agricultural land and food security due to population growth, the declination in the cropland area per capita, and agricultural land degradation (Alfiky et al., 2012; FAO, 2020).

In these circumstances, about 10 billion ha is needed to sustain global food demands by 2050 (Tilman et al., 2011; Gomiero, 2016). Due to the above situation, there is a pressing need to augment the agriculture production by reclaiming the arable lands and developing new technologies for food production. In this context, several studies (Table 1) analyzed the agricultural land areas and its expansion particularly in developing countries using geospatial technologies based on different approaches.

Egypt has a total land area of about one million square kilometers, with a total population of ~95 million people in 2017 and an annual population growth rate of 2.56% during the period 2006 - 2017(Central Agency for Public Mobilization and Statistics [CAPMAS], 2017, 2018). About ~95% of the total population lives on a small territory of the country (~ 4%) around the Nile Valley and its Delta (CAPMAS, 2019). The United Nations has estimated an increase in the population to be 123 million people by 2030 and further to 174 million people by 2050 (United Nations, 2017). Arable and fertile lands are limited to less than 4% of the total area of the country and almost all of it is irrigated (~ 98%) (FAO, 2016). In 2017, the total cultivated area was approximately 3.8 million ha including the recently reclaimed areas account for 3.82% of Egypt's area. In 2018, agricultural sector accounted for 11.5% of the GDP and absorbs about 21.6% of the labor force. Also, agricultural exports represent over 20% of the total commodity exports (CAPMAS, 2019).

Table 1. Examples of different methods appearing in the literature used for monitoring and mapping agricultural land areas and its expansion in some developing countries

Ref	Approaches
Basnet & Vodacek, 2015	Utilized Landsat TM/ETM+ over Lake Kivu region in central Africa using RF algorithm to monitor land cover change and found agricultural land had expanded from 28,730 km^2 in 1988 to 34,630 km^2 in 2011, with overall accuracies between 90.91- 94.52%.
Butt et al., 2015	Used TM and SPOT-5 HRG to detect LULC changes over Simly watershed, Pakistan. They applied MLC-based classification and found that the agricultural lands were increased from 1775 ha in 1992 to 4681 ha in 2012.
Singh et al., 2016	Employed Landsat TM and ETM+ to assess the change in LULC in lower Assam, India. MLC and NDVI-based classification have been applied. The results showed that the area of the agricultural field has increased from 3065.2 km^2 in 1990 to 3290.4 km^2 in 2014.
Knauer et al., 2017	Used Landsat (TM, ETM+, OLI) and MODIS data over Burkina Faso, West Africa. They developed an automated framework for delineating the agricultural areas using RF-based classification and found an expansion of agricultural area of 61,100 km^2 in 2001 to 116,900 km^2 in 2014, with overall accuracies between 91- 92%.
She et al., 2017	Used TM and OLI for monitoring LULC change over Dongtai County, China. They applied MLC-based classification. The results demonstrated that the agricultural fields increased from 95.7 km^2 in 1985 to 198.5 km^2 in 2010.
Youssef et al., 2019	Employed TM, ETM+ and OLI to assess the agriculture activities over Al-Jouf region, Saudi Arabia. They applied NDVI and MLC-based classification. The results showed that the agriculture land expanded from ~37.9 km^2 in 1988 to 2734.6 km^2 in 2017.
Alawamy et al., 2020	Used TM, ETM+ and OLI to detect LULC changes over Al-Jabal Al-Akhdar, Libya by applying MLC-based classification. They found that the Orchards and rain-fed agriculture lands gained 4095 ha, and the land under irrigated crops increased by 2266 ha with overall accuracy in between 81-83%.

Note: TM—Thematic Mapper; ETM+— Enhanced Thematic Mapper Plus; OLI—Operational Land Imager; SPOT-5 HRG— Satellite Pour l'Observation de la Terre 5 High Resolution Geometric; MODIS—Moderate Resolution Imaging Spectroradiometer; NDVI—Normalized Difference Vegetation Index. RF—Random Forest; LULC—Land use/Land cover; MLC—Maximum Likelihood Classifier.

The progressive increase of the population caused decreasing in the agriculture areas per capita to be 0.01 ha in 2013 compared to 0.12 ha in 1950, 0.06 ha in 1990, and 0.04 ha in 2009 (CAPMAS, 2009). This sharp decline decreased crop production per capita which directly affected the food demand at the local and country levels. The accelerated rate of the population growth prompts a high demand for food, housing, and infrastructure. Egypt is one of the largest food importers (i.e., 37% of Egypt's imports) (FAO, 2016).

Recently, the encroachment on agricultural land has become a challenging issue in Egypt and about 138,000 ha of its arable land has been lost between 1983 and 2018 due to urbanization (Ministry of Agriculture and Land Reclamation, 2018). For such challenges, Egypt has adopted a set of policies and strategies to sustain the agricultural land areas and food production through horizontal expansion and investment in land reclamation in the desert areas surrounding the green zone of the Nile Valley and its Delta. These lands have all the potential for being agriculture lands, which could effectively mitigate the conflict between land resources shortage and population needs (Abou-Hadid et al., 2010). For example, during the period 1932-1952, the reclaimed area was ~ 48,000 ha. Between 1952 and 1970, large area of ~ 383, 115 ha was reclaimed (World Bank, 1990; Ghabour et al., 2018). Since the 1990s, Egypt has established many agricultural development projects in different locations such as the Toshka project, East Owainat project, and Sinai development. In 2015, a land reclamation project of 630.000 ha in the desert was inaugurated by the Egyptian government in preparation for expected future population growth (Egypt Today, 2018; Iwasaki et al., 2021). Overall, governmental efforts successfully transformed ~1.2 million ha from desert areas to agricultural land (Bratly & Ghoneim, 2018; Radwan, 2019; CAPMAS, 2019).

Accurate and up-to-date geospatial information on LULC dynamics is critical for the sustainable development of natural resources (Basnet & Vodacek, 2015). In this context, the conventional methods such as ground surveying can provide accurate information about LULC, however, they are less effective at larger scales due to several reasons including time consumption, date lags, high costs, tedious, probability of human error, and inability to estimate and map the spatial distribution of cropland change over space and time (Hereher, 2012; El-Hattab, 2016). To overcome these issues, remote sensing and GIS would be the best alternative to study, evaluate, and analyze the spatial and temporal dynamics of land cover changes, especially over large areas (Dewan & Yamaguchi, 2009; Alam et al., 2020).

Among the various remote sensing systems, Landsat TM, ETM+, and OLI provide historical and continual global coverage at moderate to high spatial resolutions since 1972. This is adequate for mapping and monitoring land cover changes over time and vast space (Roy et al., 2014). Wadi El-Noqra (study area) did not receive proper investigation for its reclamation activities though other studies have been conducted in other geographical locations in Egypt such as Abd El-Kawy et al. (2011) employed TM and ETM+ using supervised classification-based MLC to assess LULC in a new reclaimed area in the western Nile Delta. They found that the agricultural land expanded from 11,988 ha in 1984 to 69,623 ha in 2009. In another study (Mohamed et al., 2017) OLI was utilized to monitor LULC changes in a new reclaimed area in the northwest of El-Mania Governorate. They applied MLC and NDVI analysis and found the agricultural land expanded from 3298 ha in 2014 to 4037 ha in 2017. Radwan (2019) applied MLC classification of TM, ETM+, and OLI data to monitor LULC changes over Tiba district, western Nile Delta. They found that the agricultural land had expanded from zero (0) ha in 1988 to 10,510 ha in 2018. The objective of this study was to analyze the annual spatiotemporal dynamics in a newly reclaimed area (i.e., Wadi El-Noqra) in southeastern desert, Upper Egypt, using continuous Landsat time-series images from 2005 to 2020.

Study Area

Wadi El-Noqra is located between latitudes 24° 21′ and 24° 33′ N and longitudes 33° 07′ and 33° 36′ E in the southeastern desert of Egypt within Aswan governorate (Figure 1). It covers 27874.35 ha (~278 km^2). It engulfs five villages, namely, El Manar, El Hakmah, El Amaal, El Barayem and Al

Figure 1. Geographical location of Wadi El-Noqra (the study area) in the Southeastern Desert, Upper Egypt

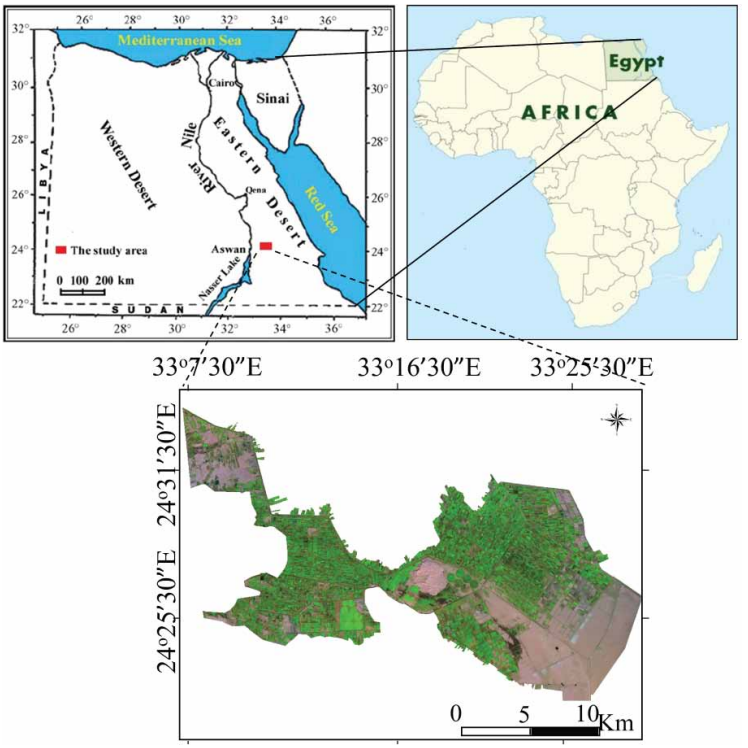

Karama. Climatically, the area is characterized by a desert climate with hot/dry summer and warm winter with rare precipitation. The mean monthly temperature varies from 17.2°C in January to 34.8°C in July. The mean monthly relative humidity ranges from 19% in June to 47% in December (Egyptian Meteorological Authority, 2020). Topographically, it has a gentle slope from east to west at about ~155 m a.s.l. It depends on irrigation water through the Wadi El-Noqra main canal which has a length of 64 km and feeds 13 sub-canals supplied from the Nile River. Some of the reclaimed areas still use the surface irrigation and some others are irrigated with drip or pivot sprinkler irrigation systems. The reclamation process in the study area includes developing the irrigation and drainage systems, road networks, and urban facilities. The study area is cultivated with several crops in winter such as wheat, barley, beans, onion, and tomato. In summer cultivated crops include sesame, peanuts, corn, mint fennel seeds, parsley, and hibiscus.

MATERIALS AND METHODS

The study adopted an integrated methodology for analyzing the spatiotemporal dynamics of agricultural land in a newly reclaimed area from 2005 to 2020. The methodology integrated the remote sensing and GIS analysis with field observations as shown in Figure 2.

Satellite Data and Its Preprocessing

Fifteen Landsat images (i.e., seven Landsat-5 TM images for 2005 to 2011 and eight Landsat-8 OLI images for 2013 to 2020). The images were acquired during the same growing season to ensure the similarity of environmental, atmospheric, and plantation cycle. The images (Table 2) were 100%

Figure 2. General methodological framework for analyzing the spatiotemporal dynamics of agriculture in a newly reclaimed area in Wadi El-Noqra, Southeastern Desert, Upper Egypt from 2005 to 2020

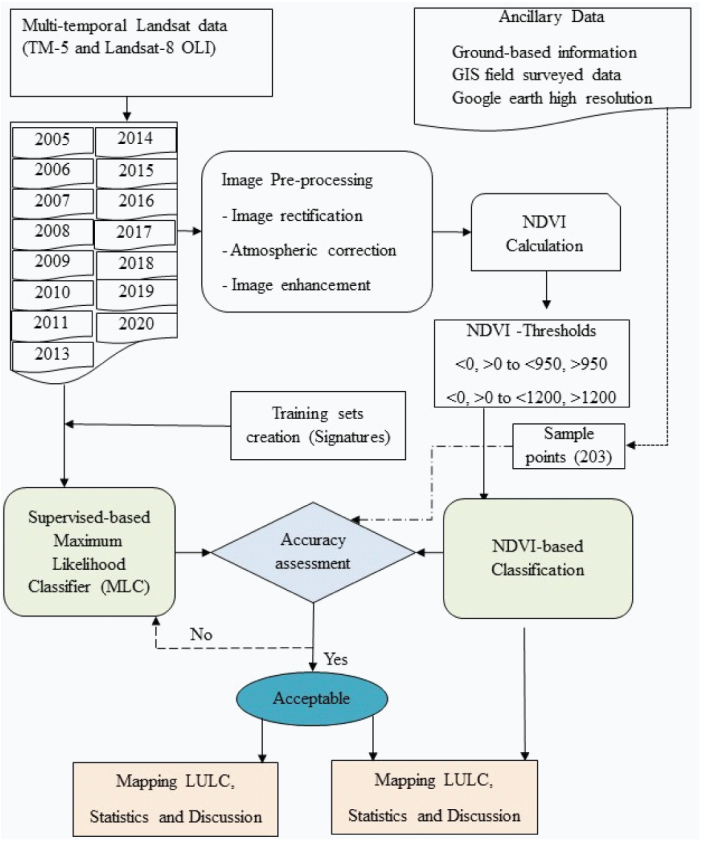

Table 2. Characteristics of the Landsat images used for analyzing the spatiotemporal dynamics of a new reclaimed area in southeastern desert, Upper Egypt (i.e., Wadi El-Noqra) during the period 2005 – 2020

Feature	Landsat TM	Landsat OLI
Spectral region and spatial resolution	VNIR 1, 2, 3, 4 (30 m) SWIR 5, 7 (30 m)	VNIR 1, 2, 3, 4, 5 (30 m) SWIR 6, 7 (30 m)
Band wavelengths (μm)	Blue: 0.45–0.52 μm Green: 0.52–0.60 μm Red: 0.63–0.69 μm NIR: 0.76–0.90 μm SWIR1: 1.55–1.75 μm SWIR2: 2.08–2.35 μm	Blue: 0.45–0.51 μm Green: 0.53–0.59 μm Red: 0.64–0.67 μm NIR: 0.85–0.88 μm SWIR1: 1.57–1.65 μm SWIR2: 2.11–2.29 μm
Acquisition dates Path: 174 Row: 43	19 November 2005 8 December 2006 22 September 2007 13 December 2008 16 December 2009 19 December 2010 3 October 2011	11 December 2013 14 December 2014 17 December 2015 19 December 2016 4 November 2017 9 December 2018 28 December 2019 14 December 2020

cloud free and were freely obtained from Google Earth Engine portal. Then subset operation has been performed using the administrative boundary of the study area. Other ancillary data were used to support the analysis such as topographic sheets (scale; 1:50,000) and field surveys for collecting the training and references samples for classification and accuracy assessment.

A spectral band composite was made for seven Landsat TM bands for each year (i.e., bands 1 through 5 and 7) and eight Landsat-8 bands (bands 1 through 7). Then, several band combinations were visually tested to select the best combination to differentiate between the LULC types. In the current study, false color combinations of SWIR, NIR, and Blue spectral bands (Figure 3) were used for visual interpretation and the selection of training sample patches to perform the MLC-classification. For the current study, LULC features were categorized into two main classes i.e., agricultural and bare lands. Agriculture lands mainly represents the cultivated field crops, vegetables, and fruit trees. Bare lands include those land surface features devoid of any type of vegetation cover including the desert areas, irrigation canals, road, and the five villages which have been constructed in the beginning of the reclamation process.

LULC Classification

Supervised Classification-Based MLC

The spatial and quantitative information in the current study was retrieved using the supervised classification-based MLC method. It was selected because of its robustness and does not require an extended training process. It relies on pixel spectral information for accurate and precise assessment of the LULC classification (Lillesand & Kiefer, 1994; Koko et al., 2021; Youssef et al., 2019). The basis of the MLC is the Likelihood of each group of pixels with similar spectral signatures to be grouped into one LULC class (Jensen, 2015). It uses a parametric statistical approach to prepare the probability density distribution functions (PDF) for each individual class (ERDAS, 1999). In this study, MLC was executed following a specific protocol of four steps: (i) the training samples for each of the LULC classes were selected from the color combination image by on-screen digitization of polygons of representative sites; (ii) the pixels with similar spectral signatures enclosed within these polygons were grouped together into one land cover class and saved; (iii) once the spectral signature

Figure 3. Landsat images RGB combination bands using the SWIR, NIR, and Blue spectral bands for the TM scenes for 2005 and 2010; and for the OLI scenes in 2015 and 2020 for Wadi El-Noqra (Path/174 and Row/43)

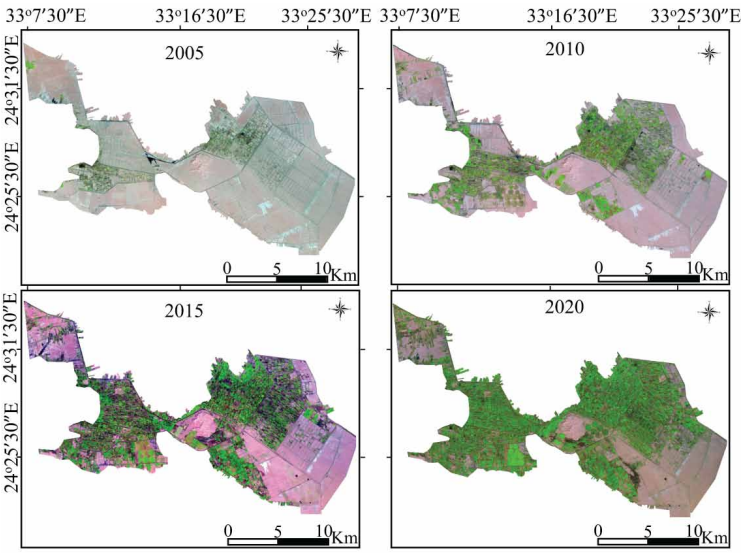

was deemed satisfactory, these spectral signature were input into the MLC without prior probability; and (iv) thematic raster layer were generated representing LULC in the study area for years 2005 to 2020. It is worthwhile to mention that a spectral signature is satisfactory when confusion in clustering of pixels among the land covers to be mapped is minimal (Geo & Liu, 2010; Butt et al., 2015).

NDVI-Based Classification

In this study, NDVI (equation 1, Rouse et al., 1974) was calculated for the 15 images from 2005 to 2020 using NIR and Red spectral bands 3 (Red, 0.63–0.69 µm) and band 4 (NIR, 0.76–0.90 µm) for Landsat TM and band 4 (Red, 0.64–0.67 µm) and band 5 (NIR, 0.85–0.88 µm) for Landsat-8 OLI. It was selected as it was successfully use for monitoring vegetation activities through utilizing the NIR and red spectral bands which are sensitive to the vegetation structure and chlorophyll activity (Wen et al., 2017; Mohamed et al., 2017). It has been shown to be highly correlated with plant health, vegetation density and cover (Ormsby et al., 1987). Also, it was used for analysis of change detection in many studies (Huang & Siegert, 2006; Xu & Guo, 2014; Singh et al., 2016; Youssef el.al., 2019) When NDVI is used to perform LULC classification is critical to define the appropriate threshold values to derive land cover classes. In doing so, each NDVI image was visually inspected to come up with specific threshold values that accurately distinguishes between land cover classes in the study area. Many points, particularly at the boundaries of agricultural lands, bare soil and built-up areas were investigated for that purpose (Figure 3):

$$NDVI = \frac{\rho NIR - \rho R}{\rho NIR + \rho R} \tag{1}$$

where, ρ *NIR* is the near infrared (NIR) band and ρ *R* is red (R) band. NDVI is a dimensionless indicator with a range between –1 to +1, where a high NDVI value represent the density/and healthy vegetation, and a lower NDVI value means sparse vegetation or no vegetation.

Due to the variation in the spectral and the radiometric resolutions between Landsat-5 and Landsat-8 OLI, we opted to use different NDVI threshold values for each sensor to classify the NDVI images. For instance, as Landsat-8 OLI has a narrower red and NIR spectral bands and higher radiometric resolution (Table 2), it produces higher NDVI values. Several studies showed that the differences between NDVI values of different satellites sensors are directly related to the differences in their spectral bandwidths and their radiometric resolution (Abuzar et al., 2014; Xu & Guo, 2014; Mancion et al., 2020).

Here, three NDVI threshold values were applied on Landsat-5 TM and Landsat-8 OLI images to classify the images from 2005 to 2020. The values of NDVI thresholds are shown in Table 3. The adequate NDVI threshold values were identified based on (i) a detailed investigation of the NDVI images corresponding to the LULC categories (ii) interpretation of the Google Earth images; (iii) checking ground truth data (points) using sites of known change and stability; (iv) verify the values for cultivated and bare land areas; and (v) knowledge of the study area characteristics. Finally, the

Table 3. Distribution of LULC classified by thresholds-based NDVI values using Landsat TM-5 and Landsat-8 (OLI)

Class Cover	Thresholds (NDVI Values-Based TM-5	Thresholds (NDVI Values-Based Landsat-8 OLI
Water	[NDVI < 0]	[NDVI < 0]
Bare land	[NDVI >0 and <=950]	[NDVI >0 and <=1200]
Agricultural land	[NDVI >950]	[NDVI >1200]

results were used to calculate the area of each class for each image and then compared to MLC-based classification result. Note that the NDVI-based classification approach complements the MLC approach as it relayed on a mathematical combination of the original spectral bands (i.e., NIR and red) which would provide more information about LULC types (Jensen, 2015).

Accuracy Assessment of MLC- and NDVI-Based Classifications

In this study, classification accuracy was empirically identified using randomly selected reference sample points which were compared against the classified images. The percentage of the correctly/erroneously labeled pixels from each class in the image was estimated. This comparison produced error matrices which represent the base of accuracy assessment process and provides detailed information of the agreement between the classification results and reference information (Congalton & Green, 2009). For each image, overall accuracy, producer's accuracy, user's accuracy, and kappa coefficient were calculated. The overall accuracy and kappa coefficient were determined using equations (2) and (3):

$$Overall\ accuracy = \frac{\sum_{i=1}^{r} x_{ii}}{x} \tag{2}$$

where, x_{ii} is the diagonal elements in the error matrix, x is the total number of samples in error matrix:

$$K = \frac{N\sum_{i=1}^{r} x_{ii} - \sum_{i=1}^{r}\left(x_{i+} * x_{+i}\right)}{N^2 - \sum_{i=1}^{r}\left(x_{i+} * x_{+i}\right)} \tag{3}$$

where, *k is* Kappa coefficient*; r* is the number of rows in the error matrix; x_{ii} is the number of observations in row *i* and column *i*; x_{i+} and x_{+i} are the marginal totals of row *i* and column *i* respectively; and *N* is the total number of observations (pixels) (Jensen, 2005). Kappa value of 1 indicates perfect agreement and values less than 1 imply less than perfect agreement. Values lower than 0.4 represent poor agreement, values from 0.4 to 0.55 represent fair agreement, values from 0.55 to 0.7 represent good agreement, values from 0.7 to 0.85 represent very good agreement, and values higher than 0.85 represent excellent agreement (Monserud & Leemans, 1992) . The accuracy assessment was performed using 203 reference points calculated based on binomial probability theory using equation (4) and spatially distributed using a stratified random scheme to represent the land cover classes of the study area:

$$N = \frac{z^2 * p * q}{E^2} \tag{4}$$

where, *N* is the sample size, *p* is the expected percent accuracy of the entire map, *q*=100-*p*, *E* is the allowable error, and $Z = 2$.

RESULTS AND DISCUSSION

MLC and NDVI-Based Classifications

Analysis of Landsat images for each date indicated that the most observed land cover in the current study area are agriculture land and bare land. Figures 4 and 5 show the spatiotemporal dynamics in land cover using supervised classification-based MLC and NDVI-based classifications respectively.

Figure 4. Time series thematic maps of the spatiotemporal dynamics of land reclamation for selected years between 2005 and 2020 in Wadi El-Noqra, Upper Egypt using the MLC-based classification

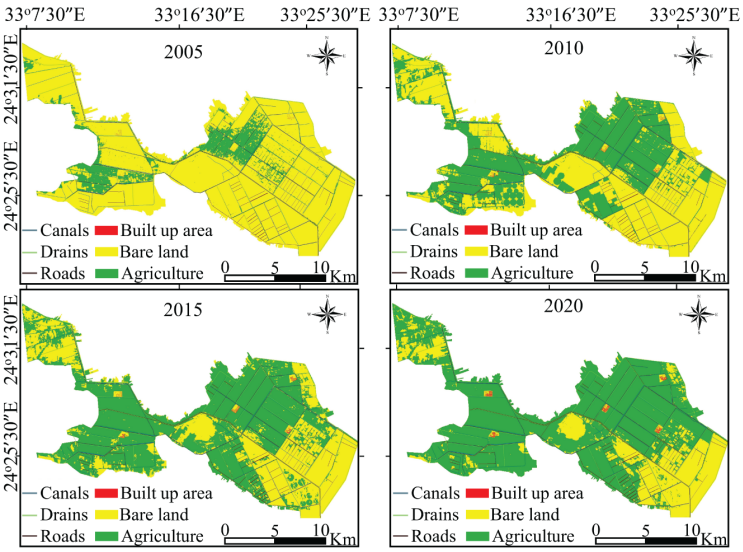

Figure 5. Time series thematic maps of the spatiotemporal dynamics of land reclamation for selected years between 2005 and 2020 in Wadi El-Noqra, Upper Egypt using the NDVI-based classification

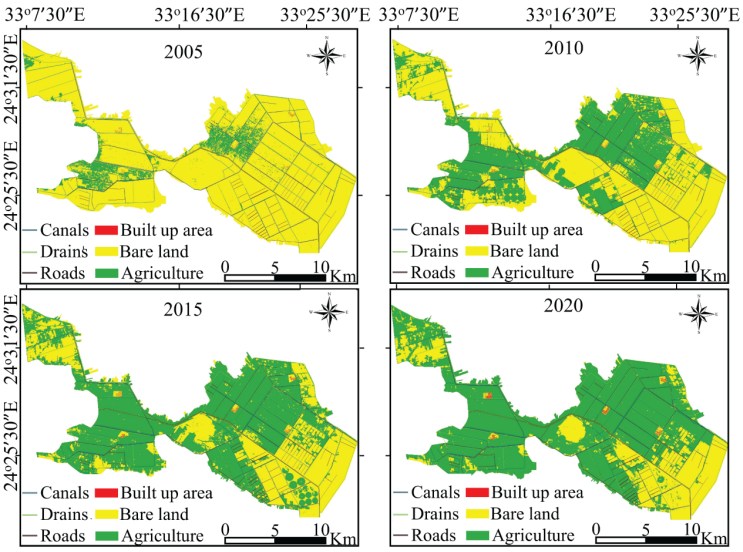

Table 4 summarizes the individual class area and change percentages for selected years between 2005-2020 for Wadi El-Noqra area.

Bare land was the dominant land cover type practically in 2005, 2006, 2007, and 2008, though, high reclamation activities were made. For the MLC method, the area of the bare land in these years were 86.6% (24136.65 ha), 80.9% (22556.791 ha), 76.4% (21297.33 ha), and 65.1% (18147.06 ha), respectively. After 2008, the development in agricultural activities continued gradually to reach approximately 66.2% (18464.6 ha) of the total area in 2015. Similar trends of agricultural land

Table 4. The area coverage in hectares and percentage for agriculture and bare land for selected years between 2005 to 2020 using MLC- and NDVI-based classifications for the study area

Year	Land Cover Classes-Based MLC and NDVI Methods								Total
	Agriculture/ha		%		Bare land/ha		%		
	MLC	NDVI	MLC	NDVI	MLC	NDVI	MLC	NDVI	
2005	3737.7	3556.81	13.4	12.8	24136.65	24317.54	86.6	87.2	27874.35
2010	12249.1	12233.8	43.9	43.9	15625.25	15640.55	56.1	56.1	27874.35
2015	18464.6	18014.8	66.2	64.6	9409.75	9859.55	33.8	35.4	27874.35
2020	20765.4	20530.3	74.5	73.7	7108.95	7344.05	25.5	26.3	27874.35

development were observed until 2020 where the agricultural land had increased to cover 74.5% (20765.4 ha) of the total area. The net percentage of changes during the whole period of study (i.e., 2005-2020) indicated that the total increase in the geographic extent of agricultural lands was approximately 455.6% (17027.7 ha) in the study area. The analysis of NDVI-based classification showed similar results, however, the MLC-based classification revealed higher values in the areas of agriculture class in all 15 images.

Classification Accuracy Assessment

Tables 5 and 6 summarize the accuracy measures of the MLC and NDVI-based classifications, respectively. The overall accuracies of MLC ranged between 95% to 97%, while the overall accuracies of the NDVI-based classification ranged between 94% to 97%. Thus, MLC provided slightly improved overall accuracies in comparison to NDVI-based classification.

The overall accuracy was greater than 85% which is satisfactory classification accuracy level of remotely sensed data for LULC mapping using Landsat imageries (Manandhar et al., 2009). Kappa Coefficient values were found between 0.88 to 0.92 for MLC and in the range of 0.86 to 0.89 for the classified images produced from NDVI-based classification. The Kappa Coefficient values were found satisfactory and falls within the range of very good to excellent agreement between images. The producer's and user's accuracies of both MLC and NDVI-based classifications showed high percentages (in the range of 86% to 98%) in the agriculture land and bare land classes. These highly accurate values might be due to several reasons including the spectral separability between the newly reclaimed lands and bare land, thus, there were minimal effects of mixed pixels between the classes. However, some errors were found in the classification results of both methods. This might be referred to several reasons including the quality of pre-processing, calibration, the type of Landsat images, and radiometric correction of the images (Phiri & Morgenroth, 2017).

Analysis of the Stages of Land Reclamation in the Study Area

The analysis of the spatiotemporal dynamics in agricultural land using both classification methods revealed three stages of agricultural developments (Figure 6) such as (i) fast and high growth rate (i.e., > 20%) between the years 2006, 2007, and 2008. This stage was characterized by fast growth rate of the agriculture activities in the study area where people and investors were assigned their land properties for agriculture investment and received the required supplies and incentives for agriculture activities; (ii) medium growth rate during the years 2009 to 2013. This stage showed less growth rates (i.e., 5-20%) compared to the first stage, however, the reclamation process tends to continue toward developing new agricultural lands according to reclamation plan; and (iii) slow and stable growth rate during the years 2014 to 2020, this stage demonstrated stable growth rate at approximately 3%. In this stage, there were some problems facing the agricultural development and productivity aspects in the study area. To determine these problems in achieving positive economic and social returns in

Table 5. Error matrices for supervised-based MLC classified images in the study area for selected years between 2005-2020

	LULC Classes	Reference Data		Producer's Accuracy (%)	User's Accuracy (%)	Overall Accuracy	Kappa Value
		Agriculture	Bare Land				
2005 Classified data	Agriculture	26	3	0.90	0.90		
	Bare Land	3	171	0.98	0.98		
						97	0.88
2010 Classified data	Agriculture	61	5	0.94	0.92		
	Bare Land	4	133	0.96	0.97		
						96	0.90
2015 Classified data	Agriculture	90	5	0.97	0.95		
	Bare Land	3	105	0.95	0.97		
						96	0.92
2020 Classified data	Agriculture	101	6	0.96	0.94		
	Bare Land	4	92	0.94	0.96		
						95	0.90

Table 6. Error matrices for NDVI-based classified images in the study area for selected years between 2005-2020

	LULC Classes	Reference Data		Producer's Accuracy (%)	User's Accuracy (%)	Overall Accuracy	Kappa Value
		Agriculture	Bare Land				
2005 Classified data	Agriculture	25	3	0.86	0.89		
	Bare Land	4	171	0.98	0.98		
						97	0.86
2010 Classified data	Agriculture	61	5	0.91	0.92		
	Bare Land	6	131	0.96	0.95		
						95	0.88
2015 Classified data	Agriculture	89	6	0.95	0.94		
	Bare Land	5	103	0.94	0.95		
						95	0.89
2020 Classified data	Agriculture	100	7	0.95	0.93		
	Bare Land	5	91	0.93	0.95		
						94	0.88

that newly reclaimed area, several field visits were paid to the study area to enumerate these problems. An in-depth personal interview and questionnaires were specially conducted on a sample of farmers and beneficiaries in Wadi El-Noqra area during the season 2019-2020. Based on the perspective of the respondents, the main-problems are: (i) lack of surface water and insufficient water-raising pumps; (ii) high prices of fertilizers, pesticides, and seeds; (iii) high fuel and transportation costs; (iv) soil salinization; and (v) some lands left unused (idle). These reasons limited the achievement

Figure 6. Graphs showing the growth rate and area of annual reclaimed land between 2005 and 2020 in Wadi El-Noqra, Upper Egypt using the MLC and NDVI

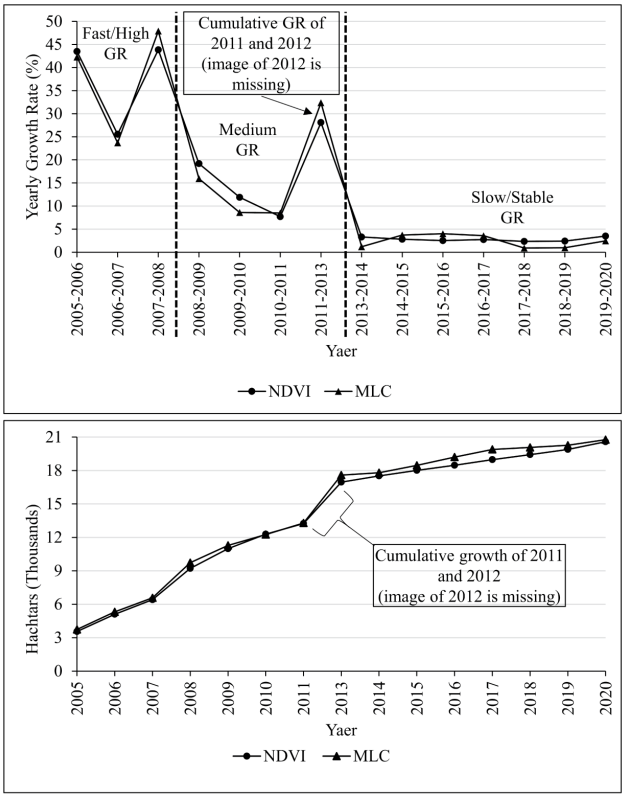

of the initial full reclamation plan which aimed to develop 27874/ha by 2020; however, only 20765/ha was reclaimed. This represents approximately 74.5% of the initial plan.

CONCLUSION AND RECOMMENDATIONS

In the present study, remotely sensed data in combination with GIS have been used for monitoring and mapping the spatiotemporal dynamics of the land reclamation activities in Wadi El-Noqra, Upper Egypt. Multi-date remotely sensed data could be of the utmost importance in combination with scheduled field visits. Both MLC and NDVI-based classification were implemented to monitor the annual land cover changes during the period of 2005 to 2020. The findings showed significant increase in the spatial extent of agriculture land to cover approximately 74.5% of the total area of Wadi El-Noqra by 2020. The LULC map using the developed methodology fulfils two important requirements: first, it differentiated and identified the LULC classes in sufficient details; second, it fulfils accuracy requirements, with most of the classes showing overall accuracy more than 94%, and user's and producer's accuracy of more than 86%, with Kappa value of more than 0.86.

Three reclamation stages were observed during the study period i.e., fast/high reclamation during the first three years (2005-2008), medium reclamation (2009-2012), and low/stable reclamation (2013-2020). During the last stage, several issues were reported and hindered the achievement of the overall goal of the reclamation plan in the study area. These included water supply, technical, cost, and land quality degradation related issues. This requires intensive and continuous revisions and monitoring

of the reclamation activities and plan in the study area. Meanwhile, the reclamation activities in the study area have several implications on the local ecosystem and the people as they changed the land cover from desert bare land into agricultural land, also they have changed the activates of the people to agriculture as owners of land which contributed to their income and quality of life.

Based on the findings, the following recommendation can be concluded (i) implementing appropriate LUCL management strategies to avoid any possible misuse by anthropogenic activities; (ii) evaluating the soil status such as soil salinity and fertility; (iii) performing a proper environmental impact assessment in the study area prior to any further development projects; (vi) monitoring groundwater management system to reduce the water consummation and accelerate agriculture development; (v) providing social services and empowerment activities to local communities to the best practices of land reclamation activities; and (iv) establishing powerful irrigation management system to sustain the water usage for future expansion in the agricultural activities. Conclusively, the results of this study would provide useful information to policy makers for further planning, developing, and monitoring the sustainable agricultural plans.

ACKNOWLEDGMENT

The authors would like to thank United States Geological Survey (USGS) for providing the multi-temporal Landsat data of the study area, free of charge. Also the authors would like to express their appreciation for the anonymous reviewers whose comments have helped to improve the overall quality of this research.

CONFLICT OF INTEREST

The authors declare there is no conflict of interest.

FUNDING

This research received no specific grant from any funding agency in the public, commercial, or not for-profit section.

REFERENCES

Abd El-Kawy, O. R., Rød, J. K., Ismail, H. A., & Suliman, A. S. (2011). Land use and land cover change detection in the Western Nile Delta of Egypt using remote sensing data. *Applied Geography (Sevenoaks, England)*, *31*(2), 483–494. doi:10.1016/j.apgeog.2010.10.012

Abou-Hadid, A. F., Abdrabbo, M. A. A., Khalil, A. A., & Hassanein, M. K. (2010). Monitoring land cover in the new reclaimed area: A case study in El-Nubaria, Egypt. *Nature and Science of Sleep*, *8*(12), 115–122.

Abuzar, M., Sheffield, K., Whitfield, D., O'Connell, M., & McAllister, A. (2014). Comparing inter-sensor NDVI for the analysis of horticulture crops in South Eastern Australia. *American Journal of Remote Sensing*, *2*(1), 1–9. doi:10.11648/j.ajrs.20140201.11

Alam, A., Bhat, M. S., & Maheen, M. (2020). Using Landsat satellite data for assessing the land use and land cover Change in Kashmir Valley. *GeoJournal*, *85*(6), 1529–1543. doi:10.1007/s10708-019-10037-x

Alawamy, J. S., Balasundram, S. K., Hanif, A. H. M., & Sung, C. T. B. (2020). Detecting and analyzing land use and land cover changes in the Region of Al-Jabal Al-Akhdar, Libya using time-series Landsat data from 1985 to 2017. *Sustainability*, *12*(11), 4490. doi:10.3390/su12114490

Alfiky, A., Kaule, G., & Salheen, M. (2012). Agricultural fragmentation of the Nile Delta; a modeling approach to measuring agricultural land deterioration in Egyptian Nile Delta. *Procedia Environmental Sciences*, *14*, 79–97. doi:10.1016/j.proenv.2012.03.009

Basnet, B., & Vodacek, A. (2015). Tracking land use/land cover dynamics in cloud prone areas using moderate resolution satellite data: A case study in Central Africa. *Remote Sensing (Basel)*, *7*(6), 6683–6709. doi:10.3390/rs70606683

Bratly, K., & Ghoneim, E. (2018). Modeling urban encroachment on the agricultural land of the eastern Nile Delta using remote sensing and GIS-based Markov Chain model. *Land (Basel)*, *7*(4), 114. doi:10.3390/land7040114

Butt, A., Shabbir, R., Ahmad, S. S., & Aziz, N. (2015). Land use change mapping and analysis using remote sensing and GIS: A case study of Simly Watershed, Islamabad, Pakistan. *The Egyptian Journal of Remote Sensing and Space Sciences*, *18*(2), 251–259. doi:10.1016/j.ejrs.2015.07.003

CAPMAS. (2009). Statistical Year book. Annual Report July 2009. Central Agency for Public Mobilization and Statistics—Arab Republic of Egypt, Cairo, Egypt.

CAPMAS. (2017). General census of population, housing and establishment, Egypt Census 2017. Central Agency for Public Mobilization and Statistics—Arab Republic of Egypt, Cairo, Egypt.

CAPMAS. (2018). Egypt in figures, 2018. Central Agency for Public Mobilization and Statistics—Arab Republic of Egypt, Issues March, Ref. No. 71-01112-2018. Cairo, Egypt.

CAPMAS. (2019). *Statistical Yearbook 2019*. Central Agency for Public Mobilization and Statistics—Arab Republic of Egypt, Issue No. (110), Ref. No. 71-01111-2019.

Congalton, R. G., & Green, K. (2009). Assessing the accuracy of remotely sensed data: Principles and practices. *International Journal of Applied Earth Observation and Geoinformation*, *11*(6), 448–449. doi:10.1016/j.jag.2009.07.002

Dewan, A. M., & Yamaguchi, Y. (2009). Land use and land cover change in Greater Dhaka, Bangladesh: Using remote sensing to promote sustainable urbanization. *Applied Geography (Sevenoaks, England)*, *29*(3), 390–401. doi:10.1016/j.apgeog.2008.12.005

Egypt Today. (2018). *A look at the national project for reclamation and cultivation*. Available online: https://www.egypttoday.com/Article/3/62373/A-look-at-the-National-Project-for-Reclamation-and-Cultivation

Egyptian Meteorological Authority. (2020). *Annual and Monthly meteorological reports*.

El-Hattab, M. M. (2016). Applying post classification change detection technique to monitor an Egyptian coastal zone (Abu Qir Bay. *The Egyptian Journal of Remote Sensing and Space Sciences*, *19*(1), 23–36. doi:10.1016/j.ejrs.2016.02.002

ERDAS. (1999). *ERDAS Field Guide, Revised and Expanded* (15th ed.). ERDAS, Inc.

FAO. (2016). *AQUASTAT country profile – Egypt*. Food and Agriculture Organization of the United Nations (FAO). Rome, Italy. Available online: https://www.fao.org/3/i9729en/I9729EN.pdf

FAO. (2020). *World food and agriculture-statistical Yearbook 2020*. 10.4060/cb1329en

Geo, J., & Liu, Y. (2010). Determination of land degradation causes in Tongyu county Northeast China via land cover change detection. *International Journal of Applied Earth Observation and Geoinformation*, *12*(1), 9–16. doi:10.1016/j.jag.2009.08.003

Ghabour, T. K., Aziz, A. M., & Rahim, I. S. (2018). land evaluation of old and recent cultivated reclaimed desert sandy soils in Egypt. *Bioscience Research*, *15*(3), 1787–1795.

Gomiero, T. (2016). Soil degradation, land scarcity and food security: Reviewing a complex challenge. *Sustainability (Basel)*, *8*(3), 281. doi:10.3390/su8030281

Hereher, M. E. (2012). Analysis of urban growth at Cairo, Egypt using remote sensing and GIS. *Natural Science (Irvine, Calif.)*, *4*(6), 355–361. doi:10.4236/ns.2012.46049

Huang, S., & Siegert, F. (2006). Land cover classification optimized to detect areas at risk of desertification in North China based on spot vegetation imagery. *Journal of Arid Environments*, *67*(2), 308–327. doi:10.1016/j.jaridenv.2006.02.016

Iwasak, E., Negm, A. M., & Elbeih, S. F. (2021). Sustainable water solution in the western desert, Egypt: Dakkla Oasis, Earth and Environment Sciences Library. Springer Natural Switzerland AG.

Jensen, J. R. (2005). *Introductory digital image processing: A remote sensing perspective* (3rd ed.). Prentice Hall.

Jensen, J. R. (2015). *Introductory Digital Image Processing: A Remote Sensing Perspective* (4th ed.). Prentice Hall.

Knauer, K., Gessner, U., Fensholt, R., Forkuor, G., & Kuenzer, C. (2017). Monitoring agricultural expansion in Burkina Faso over 14 years with 30m resolution time series: The role of population growth and implications for the environment. *Remote Sensing (Basel)*, *9*(2), 132. doi:10.3390/rs9020132

Koko, A. F., Wu, Y., Abubakar, G. A., Alabsi, A. A. N., Hamed, R., & Bello, M. (2021). Thirty years of land use/land cover changes and their impact on urban climate: A study of Kano Metropolis, Nigeria. *Land (Basel)*, *10*(11), 1106. doi:10.3390/land10111106

Lillesand, T. M., & Kiefer, R. W. (1994). *Remote Sensing and Photo Interpretation* (3rd ed.). John Wiley and Sons.

Manandhar, R., Odeh, I. O. A., & Ancev, T. (2009). Improving the accuracy of land use and land cover classification of Landsat data using post-classification enhancement. *Remote Sensing (Basel)*, *1*(3), 330–344. doi:10.3390/rs1030330

Mancion, G., Ferrara, A., Padula, A., & Nolè, A. (2020). Cross-comparison between Landsat-8 (OLI) and Landsat 7 (ETM+) derived vegetation indices in a Mediterranean environment. *Remote Sensing (Basel)*, *12*(2), 291. doi:10.3390/rs12020291

Ministry of Agriculture and Land Reclamation. (2018). *Encroachments on agricultural lands from 1983 to 2018. Ministry of Agriculture and Land Reclamation*. MALR.

Mohamed, A. H., Mahmoud, A. G., Shendi, M. M., & Awadalla, A. A. (2017). Monitoring of land reclamation development in newly reclaimed area in El-Mania Governorate, Egypt. *International Journal of Environment & Agricultural Science*, *1*(2), 1–8.

Monserud, R. A., & Leemans, R. (1992). Comparing global vegetation maps with the Kappa statistic. *Ecological Modelling*, *62*(4), 275–293. doi:10.1016/0304-3800(92)90003-W

Ormsby, J. P., Choudhury, B. J., & Owe, M. (1987). Vegetation spatial variability and its effect on vegetation indices. *International Journal of Remote Sensing*, *8*(9), 1301–1306. doi:10.1080/01431168708954775

Phiri, D., & Morgenroth, J. (2017). Developments in Landsat land cover classification methods: A review. *Remote Sensing (Basel)*, *9*(9), 967. doi:10.3390/rs9090967

Pimentel, D., & Burgess, M. (2013). Soil erosion threatens food production. *Agriculture*, *3*(3), 443–463. doi:10.3390/agriculture3030443

Radwan, T. M. (2019). Monitoring agricultural expansion in a newly reclaimed area in the Western Nile delta of Egypt using Landsat imageries. *Agriculture*, *9*(7), 137. doi:10.3390/agriculture9070137

Rouse, J. W., Haas, R. H., Schell, J. A., Deering, D. W., & Harlan, J. C. (1974). *Monitoring the vernal advancements and retrogradation (Green Wave Effect) of nature vegetation. NASA/GSFC Final Report*. NASA.

Roy, D. P., Wulder, M. A., Loveland, T. R., Woodcock, C. E., Allen, R. G., Anderson, M. C., Helder, D., Iron, J. R., Johnson, D. M., Kennedy, R., Scambos, T. A., Schaaf, C. B., Schott, J. R., Sheng, Y., Vermote, E. F., Belward, A. S., Bindschadler, R., Cohen, W. B., Geo, F., & Hipple, J. D. et al. (2014). Landsat-8: Science and product vision for terrestrial global change research. *Remote Sensing of Environment*, *145*, 154–172. doi:10.1016/j.rse.2014.02.001

She, J., Guan, Z., Cai, F., Pu, L., Tan, J., & Chen, T. (2017). Simulation of land use changes in a coastal reclaimed area with dynamic shorelines. *Sustainability (Basel)*, *9*(3), 431. doi:10.3390/su9030431

Singh, R. P., Singh, N., Singh, S., & Mukherjee, S. (2016). Normalized difference vegetation index (NDVI) based classification to assess the change in land use/land cover (LULC) in lower Assam, India. *International Journal of Advanced Remote Sensing and GIS*, *5*(10), 1963–1970. doi:10.23953/cloud.ijarsg.74

Tilman, D., Balzer, C., Hill, J., & Befort, B. L. (2011). Global Food demand and the sustainable intensification of agriculture. *Proceedings of the National Academy of Sciences, 108*(50), 20260-20264. doi:10.1073/pnas.1116437108

United Nations. (2017). *World population prospects: The 2017 Revision*. Department of economic and social affairs, population division, 2017. Available online: https://population.un.org/wpp/

Wen, Z., Wu, S., Chen, J., & Lü, M. (2017). NDVI indicated long-term interannual changes in vegetation activities and their response to climate and anthropogenic factors in the three Gorges Reservoir Region, China. *The Science of the Total Environment*, *574*, 947–959. doi:10.1016/j.scitotenv.2016.09.049 PMID:27665454

World Bank. (1990). *Land reclamation subsector review, Arab Republic of Egypt, Europe, Middle East and North Africa Region*. Country Department III, Agriculture Operations Division, Report No.8047-EGT.

World Bank. (2020). *Employment in agriculture*. Available online: https://data.worldbank.org/indicator/SL.AGR.EMPL.ZS

World Bank. (2021). *Agriculture and Food.* Available online: https://www.worldbank.org/en/topic/agriculture/overview

Xu, D., & Guo, X. (2014). Compare NDVI extracted from Landsat-8 imagery with that from Landsat 7 imagery. *American Journal of Remote Sensing*, *2*(2), 10–14. doi:10.11648/j.ajrs.20140202.11

Youssef, A. M., Abu Abdullah, M. M., Pradhan, B., & Gaber, A. F. D. (2019). Agriculture sprawl assessment using multi-temporal remote sensing images and its environmental impact; Al-Jouf, KSA. *Sustainability (Basel)*, *11*(15), 4177. doi:10.3390/su11154177

Mostafa Mosleh holds a Ph.D. degree in GIS and Land Tenure from the Department of Geomatics Engineering at the University of Calgary in Canada in 2015. He received his master's degree in rural settlement using GIS and Remote Sensing applications from the Department of Geography at South Valley University in Egypt in 2005. He also received a BA in Geography from Cairo University-Beni Suef branch in Egypt in 1997. His research primarily focuses on using remote sensing and Geographic Information Systems (GIS) for geographical studies, processing and analysis of geospatial data, the examination of land use/land cover changes, and environmental modeling. Dr. Mostafa has taught several courses including, urban geography, rural settlement, GIS, remote sensing.

Khaled Mohmmad Amin Hazaymeh holds a PhD degree in Earth Observation from the Department of Geomatics Engineering in University of Calgary/Canada in 2016. He received his master's degree in Remote Sensing and GIS from geomatics unit of the faculty of engineering in University Putra Malaysia (UPM) in Malaysia in 2008 and BA in Geography/Spatial planning from Yarmouk University in Jordan in 2004. His research interests include developing remote sensing and mapping techniques, environmental modelling, and civilian applications of remote sensing. Dr. Hazaymeh has taught several GIS, and remote sensing.